

## Synthesis of Porous Fiber-like $\text{CoMn}_2\text{O}_4$ Derived from Cotton Template as Lithium Ion Battery Anodes

Chenhao Zhao\*, Bojun Peng

College of Chemistry & Materials, LongYan University, Fujian LongYan, 364012, China.  
Fujian Provincial Key Laboratory of Clean Energy Materials, LongYan University, Fujian LongYan, 364012, China.

\*E-mail: [zhaochenhao123456@163.com](mailto:zhaochenhao123456@163.com)

Received: 19 October 2017 / Accepted: 13 december 2017 / Published: 28 December 2017

---

Porous fiber-like  $\text{CoMn}_2\text{O}_4$  has been prepared by a cotton template route. The fiber-like  $\text{CoMn}_2\text{O}_4$  with hausmannite-type structure is composed of numerous nanoparticles with an average size of ~100 nm. A Brunauer-Emmett-Teller (BET) surface area of  $12.28 \text{ m}^2 \text{ g}^{-1}$  and mesoporous structure can be calculated from  $\text{N}_2$  adsorption-desorption isotherms for porous fiber-like  $\text{CoMn}_2\text{O}_4$ . As anode of lithium ion battery, the  $\text{CoMn}_2\text{O}_4$  obtained from  $600^\circ\text{C}$  shows a reversible discharge capacity of  $867.0 \text{ mAh g}^{-1}$  and a capacity retention ratio of 86.8% after 60 cycles at a current rate of  $200 \text{ mA g}^{-1}$ . Even at a high rate of  $1 \text{ A g}^{-1}$ , the sample still delivers a stable discharge capacity of  $546.0 \text{ mAh g}^{-1}$ . These promising electrochemical performances could be attributed to the unique porous fiber structure of  $\text{CoMn}_2\text{O}_4$ .

---

**Keywords:** Cotton template, porous fiber-like  $\text{CoMn}_2\text{O}_4$ , lithium ion battery, anode materials.

### 1. INTRODUCTION

The ever-growth demand of high-performance lithium ion batteries (LIBs) have caused increased attentions in advanced electrode materials. As one of most promising anode materials for LIBs, conversion-type transition metal oxides ( $\text{MnO}_x$ ,  $\text{Co}_3\text{O}_4$  and  $\text{FeO}_x$ ) have been given tremendous attention due to their high theoretic capacities ( $500\sim 1000 \text{ mAh g}^{-1}$ ) compared with currently-used graphite ( $372 \text{ mAh g}^{-1}$ ) [1-5]. However, the conversion-type electrode materials undergo a serious volume change and poor electron (or Li-ion) conductivity during Li ion insertion and extraction process. In order to overcome above shortages, one of alternative methods is constructing porous or hollow structural metal oxides. Therein, the existence of porous structure can effectively increase the

contact area between electrode materials and electrolyte, and buffer the volume change during cycling [6-9].

Besides, the selection of different transition metal oxides is essential. Among all transition metal oxides, the cobalt-based oxides especially spinel-structure cobalt oxides ( $\text{Co}_3\text{O}_4$  and  $\text{A}\text{Co}_2\text{O}_4$ ) can reach a practical discharge capacity of over  $1000 \text{ mAh g}^{-1}$  [10-12]. The Mn-based oxides ( $\text{MnO}_x$  or  $\text{AMn}_2\text{O}_4$ ) have a low voltage plateau and good cycling stability, which is favorable to release high energy at a whole cell [13-15]. Thus, the binary metal oxides such as  $\text{CoMn}_2\text{O}_4$  or  $\text{MnCo}_2\text{O}_4$  composed of Co and Mn elements may be promising based on the possible synergic effect of Co and Mn [16-22]. The electrochemical properties of  $\text{CoMn}_2\text{O}_4$  as anode of LIBs have been firstly investigated by Courtel et al., and the sample obtained from oxalate co-precipitation route can deliver a reversible discharge capacity of  $\sim 550 \text{ mAh g}^{-1}$  [23]. Lou et al. also report synthesis of double-shelled  $\text{CoMn}_2\text{O}_4$  hollow microcubes by a carbonate co-precipitation route. The resulting microcubes show a reversible discharge capacity of  $827 \text{ mAh g}^{-1}$ , and a capacity value of  $624 \text{ mAh g}^{-1}$  can be retained at a current density of  $200 \text{ mA g}^{-1}$  after 50 cycles [24].

The natural cellulose substances such as cotton, filter paper have been used as templates to prepare of metal oxides due to their unique 3D fiber-like structure, and the products with porous network structures at nanometer levels can be readily obtained [25, 26]. Importantly, these 3D porous metal oxides originated from the cellulose template show excellent properties in the field of catalysis and/or electrochemical energy storage [25]. In this paper, the porous fiber-like binary metal oxide  $\text{CoMn}_2\text{O}_4$  has been prepared by a facile cotton template route. The structures, morphologies and electrochemical properties of  $\text{CoMn}_2\text{O}_4$  obtained from different temperatures are comparatively investigated and discussed in the context.

## 2. EXPERIMENTAL

### 2.1 Synthesis of porous fiber-like $\text{CoMn}_2\text{O}_4$

All reagents are A.R. grade and used as received. Firstly,  $0.4822 \text{ g Co}(\text{NO}_3)_2 \cdot 6\text{H}_2\text{O}$ ,  $1.1930 \text{ g Mn}(\text{NO}_3)_2$  (50wt% in solution) and  $1.0507 \text{ g}$  citric acid are dissolved into  $10 \text{ mL}$  distill water. Then,  $0.5 \text{ g}$  absorbent cotton is immersed into above solution to completely adsorb. After drying at  $80^\circ\text{C}$  for  $\sim 24 \text{ h}$ , the cotton-metal nitrate composite can be obtained. To preparation of porous  $\text{CoMn}_2\text{O}_4$ , the composite is calcinated at a temperature of  $500, 600$  or  $700^\circ\text{C}$  for  $4 \text{ h}$  in the air.

### 2.2 Structural and morphology characterization

The crystal structures of various  $\text{CoMn}_2\text{O}_4$  are recorded by powder X-ray diffractometers (DX-2700) in a scanning rate of  $0.03 \text{ degree/s}$  within  $2\theta$  region of  $10-80^\circ$ . The morphology, size and surface structure are studied by Scanning Electron Microscope (SEM, Hitachi S-3400), Transmission Electron Microscope (TEM, JEOL JEM-2100F) and selected area electron diffraction (SAED). The specific

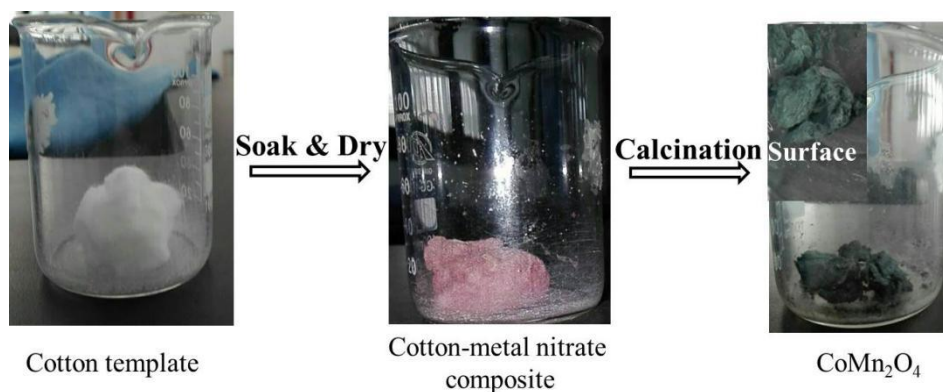
surface area and porous structure are detected by  $N_2$  adsorption-desorption isotherms, conducted in a Micromeritics sorptometer (TriStar II 3020).

### 2.3 Electrochemical study

$CoMn_2O_4/Li$  is used for electrochemical experiment in a CR 2016 coin cell at room temperature. In order to obtain the working electrode,  $CoMn_2O_4$ , acetylene black and binder sodium alginate are mixed at a weight ratio of 70 : 20 : 10. Then, the mixture is slurried by moderate amount of water, pasted on the copper foil. After drying at  $80^\circ C$  overnight, the decorated copper foil are cut into a disc with a radius of 7 mm. Commercial  $LiPF_6$  EC/DEC solution (Shenzhen Capchem) and PP film is used as electrolyte and separator, respectively. CR2016 coin cells are assembled in an Ar-filled glove box. The charge discharge tests with constant current are carried out in a CT-3008 battery test system (Shenzhen Neware) at different current densities within a voltage window of 0.01-3 V. Cyclic voltammetry (CV) measurement of  $CoMn_2O_4/Li$  is conducted in the electrochemical working station (Solartron, UK) at a scanning rate of  $0.1\text{ mV s}^{-1}$  within 0.01-3.0 V.

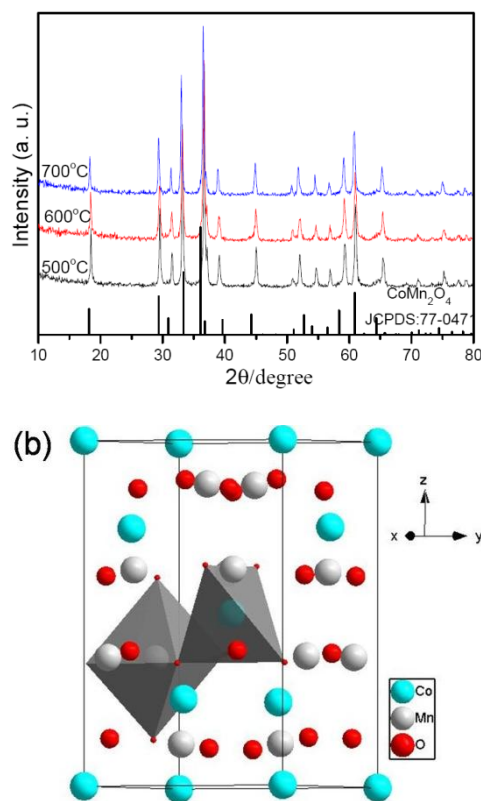
## 3. RESULTS AND DISCUSSION

### 3.1 Structural characterization



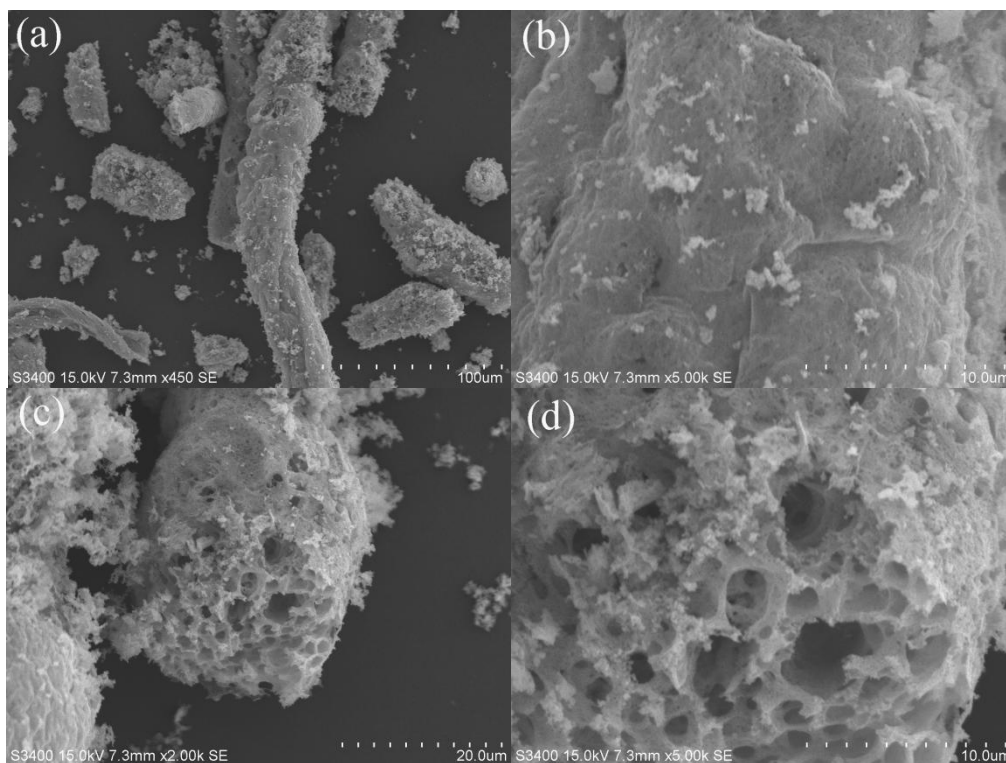
**Figure 1.** Schematic formation process of porous  $CoMn_2O_4$  form cotton template

The formation process of porous fiber-like  $CoMn_2O_4$  is schematically shown in Fig. 1. The white cotton can completely adsorb the red  $Co(NO_3)_2$ ,  $Mn(NO_3)_2$  and citric acid mixed solution. After drying at  $80^\circ C$  for  $\sim 24$  h, a red and hard cotton regiment can be obtained. This cotton regiment is immediately calcinated at a certain temperature, and the  $CoMn_2O_4$  is fabricated accompanying with removing of cotton template. Interestingly, the overall structure has not been changed except the size of regiment is reduced, as well as the color of red is transformed into dark green (Fig. 1). Some observed fiber-like structure of  $CoMn_2O_4$  can be found in the resulting product, which is similar to the cotton fiber, suggesting the successful template effect of cotton substance.



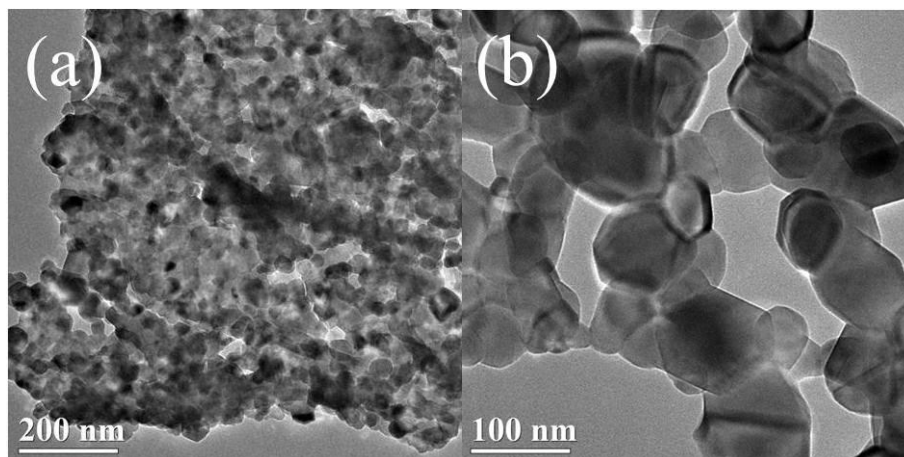
**Figure 2.** (a) XRD patterns of porous  $\text{CoMn}_2\text{O}_4$  from cotton-metal nitrate template at different calcination temperatures, (b) crystal structure of hausmannite-type  $\text{CoMn}_2\text{O}_4$ .

The loose  $\text{CoMn}_2\text{O}_4$  regiment is ground into powder in an agate mortar, which is firstly detected by XRD as shown in Fig. 2a. XRD patterns of dark green  $\text{CoMn}_2\text{O}_4$  from different temperatures can be indexed to tetragonal  $\text{CoMn}_2\text{O}_4$  (JCPDS: 77-0741), and without any impurities such as  $\text{Co}_3\text{O}_4$  or  $\text{Mn}_2\text{O}_3$  can be found, indicating the pure-phase binary metal oxides  $\text{CoMn}_2\text{O}_4$  can be prepared using cotton template route. Generally speaking, a higher calcination temperature can improve crystallinity of inorganic metal oxides. Surprised, the peak intensity of XRD pattern has not been improved along with elevated temperature (Fig. 2a). As we know, stable Co-Mn binary oxides  $\text{CoMn}_2\text{O}_4$ ,  $\text{Mn}_{1.5}\text{Co}_{1.5}\text{O}_4$  and  $\text{MnCo}_2\text{O}_4$  are tetragonal, cubic and cubic phase respectively, based on the parent structure of tetragonal  $\text{Mn}_3\text{O}_4$  and cubic  $\text{Co}_3\text{O}_4$  [27,28]. The schematic crystal structure of  $\text{CoMn}_2\text{O}_4$  is revealed in Fig. 2b, showing a hausmannite-type ( $\text{Mn}_3\text{O}_4$ ) structure, in which  $\text{Co}^{2+}$  and  $\text{Mn}^{3+}$  occupy partial tetrahedral and octahedral interstitial sites of  $\text{O}^{2-}$  in the lattice, respectively, to form  $\text{CoO}_4$  tetrahedron and  $\text{MnO}_6$  octahedron, In the structure of  $\text{CoMn}_2\text{O}_4$ , the Co has the chemical valence of +2, and it can be easily oxidized to +3. Maybe, a higher calcination temperature induces to the formation of  $\text{Co}^{3+}$ , resulting in the competitive formation of  $\text{CoO}_6$  octahedron with  $\text{MnO}_6$ , as well as decreased tetragonal structure of  $\text{CoMn}_2\text{O}_4$ .



**Figure 3.** SEM images of CoMn<sub>2</sub>O<sub>4</sub> derived from cotton template at a calcination temperature of 600°C, (a) overall view, (b) close-up view and (c, d) broken section.

Overall morphologies, size and surface structure of CoMn<sub>2</sub>O<sub>4</sub> are revealed in Fig. 3. It can be found that the CoMn<sub>2</sub>O<sub>4</sub> well inherit the fiber structure of cotton (Fig. 3a), which is consistent with the digital image in Fig. 1. On the surface of CoMn<sub>2</sub>O<sub>4</sub> fiber (Fig. 3b), some wave-like structure is clearly presented, attributing to the template effect of cotton. From the broken section of CoMn<sub>2</sub>O<sub>4</sub> fiber (Fig. 3c), numerous macropores exist in the inner of CoMn<sub>2</sub>O<sub>4</sub> fiber. In a magnification view (Fig. 3d), some particles with small size can be observed.



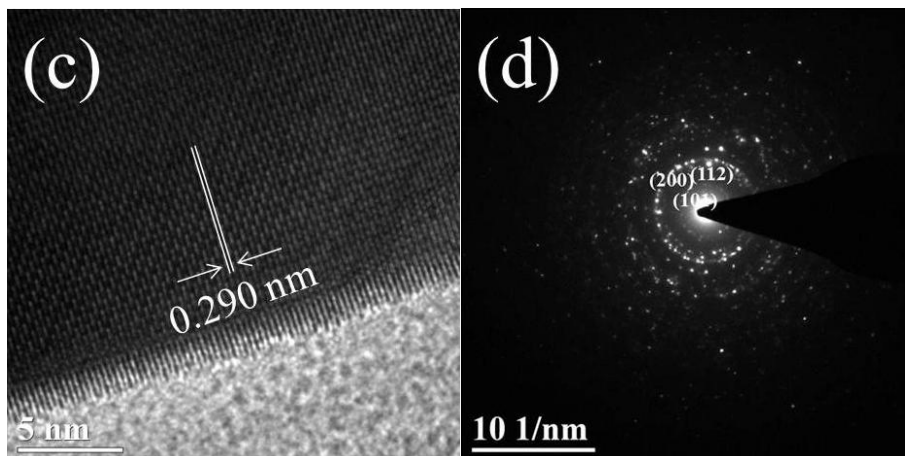


**Figure 4.** (a, b) TEM images, (c) HRTEM and (d) SAED of  $\text{CoMn}_2\text{O}_4$  derived from cotton template at a calcination temperature of  $600^\circ\text{C}$

In order to further study the structure of cotton directed  $\text{CoMn}_2\text{O}_4$ , TEM test is carried out (Fig. 4a and b). A thin plate composed of nanoparticles is successfully captured in Fig.4a, and these nanoparticles with clear corner and edge have a size of  $\sim 100$  nm. In a high resolution TEM (HR-TEM) view, a clear lattice fringe with a spacing of 0.290 nm can be indexed to the (112) crystal face of tetragonal  $\text{CoMn}_2\text{O}_4$  (JCPDS: 77-0741). From SAED pattern (Fig. 4d), some diffraction dots of (101), (200), (112) crystal face can be calculated, which can be indexed to the XRD patterns in Fig. 2a, and indicates the as-prepared  $\text{CoMn}_2\text{O}_4$  possess good crystallinity.

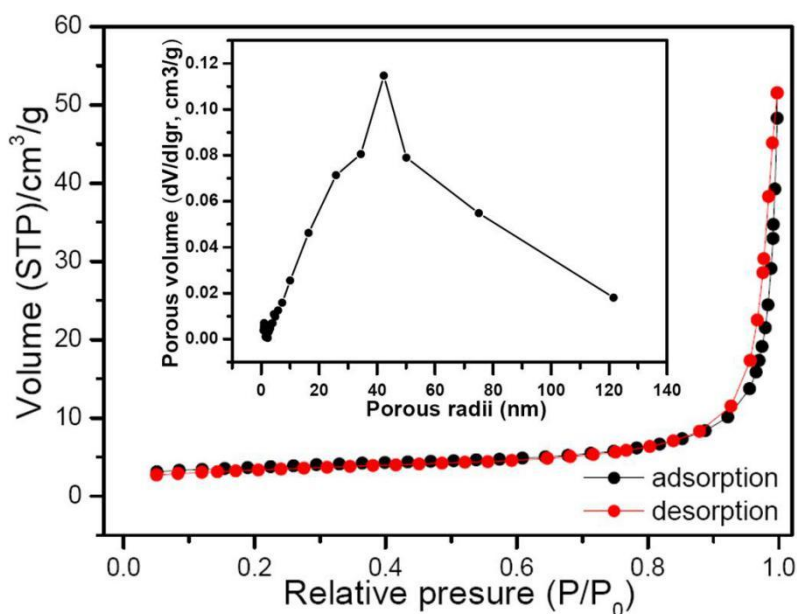


**Figure 5.**  $\text{N}_2$  adsorption-desorption isotherm and inserted pore size distribution of porous  $\text{CoMn}_2\text{O}_4$  obtained at a temperature of  $600^\circ\text{C}$ .

The porous nature is studied by  $\text{N}_2$  adsorption-desorption isotherm (Fig. 5). The isotherm shows a low adsorption amount in a low pressure, which sharply increases until the value of  $P/P_0$  reach



0.8, suggesting porous  $\text{CoMn}_2\text{O}_4$  does not contain any micro- or small- pores. The estimated Brunauer-Emmett-Teller (BET) specific surface area is  $12.28 \text{ m}^2 \text{ g}^{-1}$ , close to the  $\text{CoMn}_2\text{O}_4$  prepared from coprecipitation route [15, 26]. The inset in Fig. 5 is the pore size distribution of porous  $\text{CoMn}_2\text{O}_4$ , the pore originated from the aggregate of  $\text{CoMn}_2\text{O}_4$  nanoparticles is in the mesoporous range of 10-100 nm, keeping well with the TEM observation in Fig. 4a.

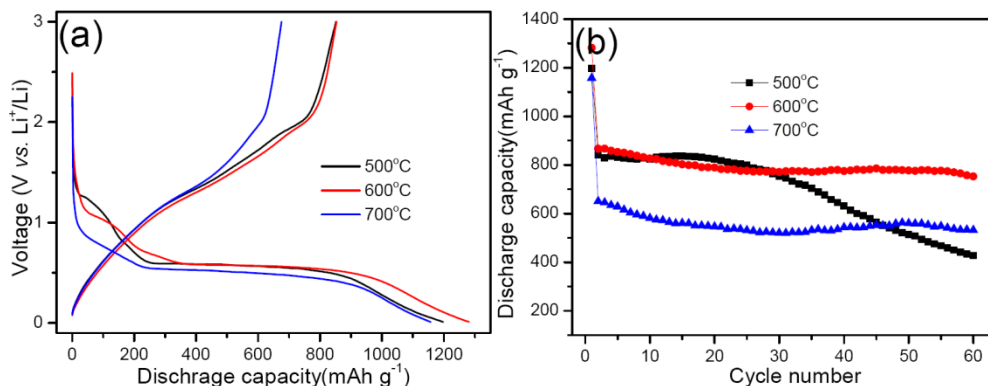


**Figure 6.** (a) Initial discharge charge curves and (b) cycle performances of  $\text{CoMn}_2\text{O}_4$  obtained from different calcination temperatures.

The electrochemical performances of conversion-type electrode materials are deeply depended upon their structures and morphologies, and the porous property may play a positive impact on the electrochemical performances of  $\text{CoMn}_2\text{O}_4$ . Fig. 6 reveals the initial discharge-charge curves and cycling performance of different  $\text{CoMn}_2\text{O}_4$ . The  $\text{CoMn}_2\text{O}_4$  from 500, 600 or 700°C reveals an initial discharge capacity of 1197.2, 1281.0 or 1157.1  $\text{mAh g}^{-1}$ , and a reversible charge capacity of 851.6, 853.2 or 675.9  $\text{mAh g}^{-1}$  can be obtained, with an initial Coulombic efficiency of 71.1, 66.7 or 58.4% (Fig. 6a). It can be found that the sample from lower temperature has a better electrochemical reversibility, which can be attributed to its smaller particle size. Cycling performance of various  $\text{CoMn}_2\text{O}_4$  is revealed in Fig. 6b, the reversible discharge capacity of 500-, 600- or 700°C- sample is 841.1, 867.0 or 650.5  $\text{mAh g}^{-1}$ . After 60 cycles at 200  $\text{mA g}^{-1}$ , a capacity of 426.8, 752.6 or 531.9  $\text{mAh g}^{-1}$  can be retained, with a capacity retention of 50.74, 86.8 or 81.8%. Obviously, the 600°C sample possesses a highest capacity retention and residual capacity. According to previous literatures, a calcination temperature of 600°C may be suitable for preparation of Mn-based binary oxides including  $\text{ZnMn}_2\text{O}_4$  and  $\text{CoMn}_2\text{O}_4$  [7, 19, 26-28].

Fig. 7 shows the initial three CV curves of  $\text{CoMn}_2\text{O}_4/\text{Li}$  cells at a scanning rate  $0.1 \text{ mV s}^{-1}$  between 0.01 and 3.0 V. In the first discharge curve, a unique intensive peak at 0.37 V is the reduction of  $\text{CoMn}_2\text{O}_4$  to metallic Mn and Co. There are two anodic peaks located at 1.33 and 1.96 V in the first charge curve, which are associated with the reversible formation of MnO and CoO, respectively. From the second cycle onward, the repeated oxidation/reduction of MnO and CoO leads to two pairs of redox peaks of 0.56/1.33 and 1.1/1.96 V, respectively. On the basis of the CV results, the entire electrochemical process can be classified as follows [16-24]:

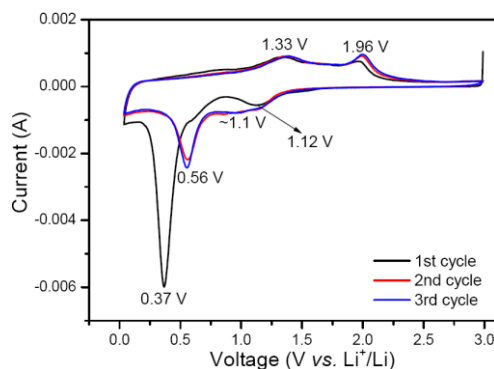
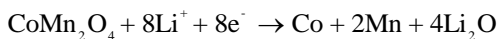


**Figure 7.** CV curves of porous fiber-like  $\text{CoMn}_2\text{O}_4$  at a scanning rate of  $0.1 \text{ mV s}^{-1}$  within 0.01-3.0 V

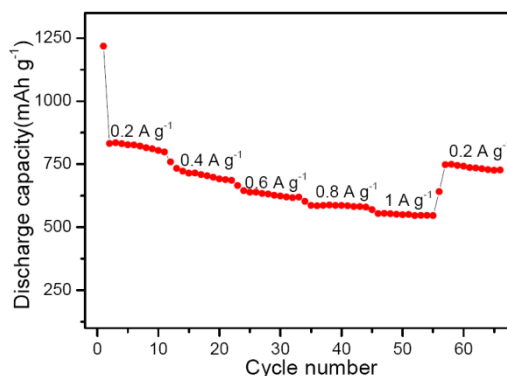


**Figure 8.** Rate capability of porous fiber-like  $\text{CoMn}_2\text{O}_4$

**Table 1.** The comparative structures and electrochemical performances of various  $\text{CoMn}_2\text{O}_4$ .

Morphology	Preparation route	Initial reversible discharge capacity ( $\text{mAh g}^{-1}$ )	Capacity retention	Rate capability ( $\text{mAh g}^{-1}$ )
Nanoparticles [23]	Oxalate precipitation	691 (0.1C)	~47.8% (50 cycles)	unknown
Hollow microcubes [24]	Carbonate precipitation	827 ( $0.2 \text{ A g}^{-1}$ )	75.5% (50 cycles)	~670 ( $0.8 \text{ A g}^{-1}$ )
Hierarchical microspheres [29]	Solvothermal	942 ( $0.1 \text{ A g}^{-1}$ )	94.9% (65 cycles)	442 (6C)
Hollow microflowers [30]	Solvothermal	729 ( $1 \text{ A g}^{-1}$ )	>100% (500 cycles)	257 ( $2 \text{ A g}^{-1}$ )
Yolk-shell [30]	solvothermal carbon template	~1355 ( $1 \text{ A g}^{-1}$ )	~53.5% (50 cycles)	711 ( $2 \text{ A g}^{-1}$ )
Hollow fiber (This work)	Template route	867 ( $0.2 \text{ A g}^{-1}$ )	86.8% (50 cycles)	546 ( $1 \text{ A g}^{-1}$ )



Rate capability is another important parameter to measure the electrochemical performance. At a current density of  $0.2 \text{ A g}^{-1}$ , a discharge capacity of  $811.3 \text{ mAh g}^{-1}$  can be obtained. When the current density is increased to  $1 \text{ A g}^{-1}$ , the electrode still delivers a stable discharge capacity of  $546.0 \text{ mAh g}^{-1}$ . Interestingly, the current density goes back to  $0.2 \text{ A g}^{-1}$  after 50 cycles, the discharge capacity is reverted to  $748.4 \text{ mAh g}^{-1}$ . These results suggest the porous fiber-like  $\text{CoMn}_2\text{O}_4$  is suitable for fast Li ions insertion/desertion process, Also, the overall electrochemical performance of this fiber-like  $\text{CoMn}_2\text{O}_4$  is not bad in comparison with other  $\text{CoMn}_2\text{O}_4$  (Tab. 1).

#### 4. CONCLUSION

We have successfully developed a facile cotton template route for the preparation of porous fiber-like  $\text{CoMn}_2\text{O}_4$ . These porous  $\text{CoMn}_2\text{O}_4$  composed of well-defined nanoparticles have good crystallinity and unique 3D porous structure. When used as lithium ion battery anodes, the porous  $\text{CoMn}_2\text{O}_4$  obtained at  $600^\circ\text{C}$  presents a high reversible discharge capacity ( $867.0 \text{ mAh g}^{-1}$ ,  $200 \text{ mA g}^{-1}$ ), good cycle stability (86.8%, 60 cycles) and rate capability ( $546.0 \text{ mAh g}^{-1}$ ,  $1 \text{ A g}^{-1}$ ). The cotton template is suitable for synthesis of porous fiber-like  $\text{CoMn}_2\text{O}_4$ , which can be used as alternative lithium ion battery anode.

#### ACKNOWLEDGEMENT

The authors thank the financial support from Scientific Start Foundation of Longyan University (LB2014001), from Provincial Science and Technology Department for Provincial Colleges and Universities Program (JK2015047).

#### References

1. P. Poizot, S. Laruelle, S. Grugeon, L. Dupont, J.M. Tarascon, *Nature*, 407 (2000) 496-499.
2. Z.Y. Wang, L. Zhou, X.W. Lou, *Adv. Mater.*, 24 (2012) 1903-1910.
3. L.X. Zeng, X.X. Huang, Q.R. Qian, M.D. Wei, *RSC Adv.*, 6 (2016) 105558-105564.
4. Y. H. Dai, H. Jiang, Y. J. Yu, C.Z. Li, *RSC Adv.*, 3 (2013) 19778-19781.
5. L.X. Liao, T. Fang, G.P. Yin, D.X. Li, B. Li, *Int. J. Electrochem. Sci.*, 12 (2017) 10211-10220.
6. Y.H. Zhang, Y.W. Zhang, C.L. Guo, Z.C Bai, *Electrochim. Acta*, 182 (2015) 1140-1144.
7. F.F. Wu, J. Bai, J.K. Feng, S.L. Xiong, *Nanoscale*, 7 (2015) 17211-17230.
8. Y.M. Sun, X.L. Hu, W. Luo, Y.H. Huang, *J. Mater. Chem.*, 22 (2012) 13826-13831.
9. Y.J. Wang, J. Ke, Y.W. Zhang, Y.H. Wang, *J. Mater. Chem. A*, 3 (2015) 24303-24308.
10. J.X. Fu, W.T. Wong, W.R. Liu, *RSC Adv.*, 5 (2015) 75838-75845.
11. J. Bai, X.G. Li, G.Z. Liu, Y.T. Qian, S.L. Xiong, *Adv. Funct. Mater.*, 24 (2014) 3012-3020.
12. G.L. Xu, J.T. Li, L. Huang, W.F. Lin, S.G. Sun, *Nano Energy*, 3 (2013) 394-402.
13. Y.F. Deng, L.N. Wang, Y. Xie, X.S. Qiu, G.H. Chen, *RSC Adv.*, 4 (2014) 23914-23935.
14. C.H. Zhao, F. Feng, X.X. Wang, R. Liu, S.Q. Zhao, Q. Shen, *Powder Technol.*, 261 (2014) 55-60.
15. G.Q. Zhang, L. Yu, H.B. Wu, H.E. Hoster, X.W. Lou, *Adv. Mater.*, 24 (2012) 4609-4613.
16. N. Garg, M. Mishra, Govind, A.K. Ganguli, *RSC Adv.*, 5 (2015) 84988-84998.
17. L.L. Yao, L.L. Zhang, Y.X. Liu, C. Wang, *CrystEngComm*, 18 (2016) 8887-8897.
18. C.C. Fu, G.S. Li, D. Luo, X.S. Huang, L.P. Li, *ACS Appl. Mater. Interfaces*, 6 (2014) 2439-2449.
19. J.F. Li, J.Z. Wang, X. Liang, Y.T. Qian, S.L. Xiong, *ACS Appl. Mater. Interfaces*, 6 (2014) 24-30.

20. M. V. Reddy, Y.M. Xu, V. Rajarajan, B. V. R. Chowdari, *ACS Sustainable Chem. Eng.*, 3 (2015) 3035-3042.
21. J.J. Yuan, C.H. Chen, Y. Hao, X.K. Zhang, Y.M. Xie, *J. Mater. Sci.*, 52 (2017) 5751-5758.
22. C.Z. Yuan, H.B. Wu, Y. Xie, X.W. Lou, *Angew. Chem. Int. Ed.*, 53 (2014) 1488-1504.
23. F. Courtel, H. Duncan, Y. Abu-Lebdeh, I. Davidson, *J. Mater. Chem.*, 21 (2011) 10206-10218.
24. L. Zhou, D.Y. Zhao, X.W. Lou, *Adv. Mater.*, 24 (2012) 745-748.
25. D.L. Jia, M.Y. Wang, S. Li, J.G. Huang, *Chin. Sci. Bull.*, 59 (2014) 1369-1381.
26. C.H. Zhao, Y. Shen, Q.E. Qiu, Z.B. Hu, K.Y. Liu, *Micro Nano Lett.*, 6 (2016) 287-290.
27. J. F. Li, S. L. Xiong, X.W. Li, Y. T. Qian, *Nanoscale*, 5 (2013) 2045-2054.
28. J.F. Li, S.L. Xiong, X.W. Li, Y.T. Qian, *J. Mater. Chem.*, 22 (2012) 23254-23259.
29. H. Lin, H. Zhong, Q.W. Chen, *Sci. Rep.*, 2 (2012) 986.
30. L.X. Zhang, G.F. Hou, H.F. Jiu, J. Qi, *J. Power Sources*, 326 (2016) 505-513.
31. L.X. Zhang, Y.L. Wang, G.F. He, *Electrochim. Acta*, 182 (2015) 550-558.

© 2018 The Authors. Published by ESG ([www.electrochemsci.org](http://www.electrochemsci.org)). This article is an open access article distributed under the terms and conditions of the Creative Commons Attribution license (<http://creativecommons.org/licenses/by/4.0/>).